This is a preprint manuscript. Please, download the final and much nicer version at:

https://dx.doi.org/10.1021/acs.analchem.8b00942

In Situ Spectroelectrochemical Monitoring of Dye Bleaching After Electrogeneration of Chlorine-Based Species. Application to Chloride Detection

Daniel Martín-Yerga[#], Alejandro Pérez-Junquera, María Begoña González-García, David Hernández-Santos, Pablo Fanjul-Bolado*.

DropSens, S.L., Ed. CEEI, Parque Tecnológico de Asturias, 33428 Llanera, Asturias, Spain.

*e-mail: pfanjul@dropsens.com; phone: +34985277685

Current address: Applied Electrochemistry, School of Engineering Sciences in Chemistry, Biotechnology and Health, KTH Royal Institute of Technology, SE 100-44 Stockholm, Sweden

ABSTRACT: Spectroelectrochemical techniques are becoming increasingly versatile tools to solve a diverse range of analytical problems. Herein, the use of *in situ* real-time luminescence spectroelectrochemistry to quantify chloride ions is demonstrated. Utilizing the bleaching effect of chlorine-based electrogenerated products after chloride oxidation, it is shown that the fluorescence of the Rhodamine 6G dye decrease proportionally to the initial chloride concentration in solution. A strong decrease of fluorescence is observed in acidic media compared to a lower decrease in alkaline media, which suggests that Cl_2, favourably generated at low pH, could be the main species responsible of the fluorescence loss. This fact is corroborated with chronoamperometric measurements where the complete loss of fluorescence for the bulk solution is achieved. A fast mass transfer is needed to explain this behavior, in agreement with the generation of gaseous species such as Cl_2. Chloride detection was performed in artificial sweat samples in less than 30 s with great accuracy. This electrochemical/optical combined approach allows to quantify species difficult to measure by electrochemistry due to the inadequate resolution of their redox processes or without significant optical properties.

Chloride levels in sweat is a relevant biomarker for the diagnostic of cystic fibrosis, a genetic chronic disease that affects mostly to lungs but also to other organs[1,2]. Chloride could also play a significant role in other diseases such as Alzheimer's[3]. There are several analytical techniques that can be used for the determination of chloride levels such as ion chromatography[4] or coulometric titration[5], but they typically require lab-scale instrumentation and complex analytical procedures. Ion-selective electrodes (ISEs)[6] have been well-established for the analytical detection of several ions such as chloride[7,8] due to their good performance and short response time. The selectivity towards specific ions is given by the membrane, but some interaction with interfering ions[9] could also happen resulting in an incorrect signal. Although this effect could be measured by using selectivity coefficients, there is still new research concerning the determination of unbiased values[10]. ISEs have also other limitations such as the difficult miniaturization because they need an inner aqueous electrolyte or their non-disposability, which makes essential to avoid the contamination of the membrane. Solid-state ISEs[11] are promising devices to replace conventional ISEs in the future, but extensive research is being performed to solve different issues with these devices[12]. Therefore, the development of new sensors with ideal characteristics for the determination of chloride is still a constant concern. A current trend is to solve analytical problems with cost-effective, miniaturized and portable devices that could be operated in the point of sample collection or decentralized venues. Optical and electrochemical methods are well placed in order to achieve simple and sensitive analysis with portable devices in Point-of-Care (POC) systems. On the one hand, optical methods can be used for chloride detection by means of a change in the optical signal after the interaction of chloride with a chemical probe. Fluorescence monitoring has been widely employed for chloride determination using probes such as fluorophores[13,14] or nanoparticles[15]. In a typical experiment, the chemical interaction of chloride with the probe changes the fluorescence intensity by producing a quenching effect[16]. On the other hand, chloride ion is electroactive but its oxidation process occurs at a very positive potential near the potential of water oxidation. Thus, it is difficult to resolve both processes and perform the quantification of chloride in a precise way by direct electrochemistry. Alternative approaches have been developed to avoid this fact such as the use of ionic liquids[17,18]. Another possibility is to indirectly detect chloride by interaction with other electroactive species such as mercury[19] or the most employed, silver[3,20,21]. The interaction chloride-metal changes the potential of the oxidation/reduction processes of the metal and some discrimination is possible. For instance, the formation of insoluble AgCl, which facilitates the oxidation of Ag^0 or inhibits the reduction of Ag^I compared to the processes involving the soluble silver species (Ag^+) has been widely employed for chloride detection. A low coverage with silver nanoparticles is typically employed, and the parameters must be extremely well-controlled in order to avoid the overlapping of the different silver processes[22], which would difficult the measurement of the analytical signal. The use of cost-effective and disposable screen-printed electrodes is a good solution in order to apply these methods in POC systems. These devices modified with silver nanoparticles have been employed

for chloride detection in synthetic sweat[23] or biological samples[24]. The change in the redox potential of indicator species in presence of chloride has also been employed for its electrochemical detection[25]. However, in some cases, the potential may be difficult to control in solid-state disposable devices using pseudoreference electrodes, which are normally fabricated with silver materials and could have some random interaction with chloride in solution, increasing the complexity of the system. Furthermore, the need of silver modification also adds some complications: the silver structure must be reproducible between devices, the nanoparticle sizes could influence the voltammetric profile[22], the stability of the silver film should be kept after storage (and silver could be easily oxidized or silver nanoparticles easily detached from the surface[26]), and the cost is also increased by using a noble metal compared to carbon electrodes.

Combining optical and electrochemical methods is a very interesting approach to enhance the information obtained from chemical systems. Spectroelectrochemistry[27] has been widely employed for the characterization of materials[28,29] or electrochromic species[30,31], kinetics studies[32], autovalidation of analytical methods[33] or the optical detection of species after electrochemical activation[34,35]. Spectroelectrochemistry is certainly promising for detecting chemical species that initially cannot be detected by the individual spectroscopic or electrochemical techniques. For instance, electrochemical surface-enhanced Raman scattering[34,36] allows the detection of species at low concentrations after the electrochemical activation of the substrate, which also helps with the adsorption of the analyte. Another possibility is to use a mediator with optical properties to detect species without these properties. Heineman et al.[37] reported the detection of ascorbate using $[Ru(bpy)_3]^{2+/3+}$ as mediator. The nonabsorbing oxidized form reacts with ascorbate and generates the reduced colored form, increasing the optical signal. The *in situ* generation of colored complexes has also been reported as a strategy to improve the detectability of chemical species[38]. In this sense, spectroelectrochemical sensors using small, cost-effective and portable devices have demonstrated a great versatility to solve different complex analytical problems with simplicity[39,40]. There are only a few examples using spectroelectrochemical techniques where halide ions play the main role of the study[41]. Although *in situ* spectroelectrochemical methods are the most interesting approach to obtain real-time transient information of chemical systems[42], *ex situ* spectroelectrochemistry has been employed in order to evaluate the degradation of dyes in presence of chloride ions[43]. These dyes, frequently used at large volumes in industrial processes, could be hazardous to the environment[44], and the electrochemical oxidation is one of the most popular methods for degrading the dye in wastewaters[45,46]. This degradation process could be achieved by indirect reactions with oxygenated radicals (in absence of chloride)[47] or by chlorine-based species (in presence of chloride)[48]. The performance of these processes is *ex situ* monitored by checking the optical properties (absorption or fluorescence) of the solutions after the electrochemical oxidation. Although the degradation process has been widely employed and numerous studies have arisen in the literature, the radically opposite approach, which is the detection of chloride after its oxidation to produce the degradation of the dyes has not been proposed.

In this work, we report the spectroelectrochemical detection of chloride by monitoring the changes of the fluorescence of R6G after the *in situ* electrogeneration of chlorine-based bleaching species. We used the well-known approach for degradation of dyes with electrogenerated chlorine species but with a radically different goal: the analytical detection of the starting species. Luminescence spectroelectrochemistry is performed with an integrated and portable instrument and cost-effective, disposable screen-printed carbon electrodes were employed for the electrochemical oxidation. The proposed method was evaluated for the detection of chloride in sweat samples, which is a biomarker of the cystic fibrosis disease. This electrochemical/optical combined approach allowed us to quantify a chemical species (chloride) with redox processes difficult to resolve and non-significant optical properties. This fact demonstrates the great ability of spectroelectrochemistry to solve complicated analytical problems in an elegant way.

EXPERIMENTAL SECTION

Instrumentation

All electrochemical, spectroscopic and spectroelectrochemical measurements were carried out with a SPELEC instrument (DropSens) controlled by DropView SPELEC software. Luminescence spectroelectrochemistry measurements were performed with a bifurcated reflection probe (DRP-FLUOPROBE, DropSens) and a specific cell for screen-printed electrodes (DRP-RAMANCELL, DropSens) working in a near-normal reflection configuration. The excitation connector of the bifurcated probe was connected to a 395 nm UV LED (DRP-UVLED, DropSens) and the detection connector of the probe was connected to the SPELEC. The LED was powered by an USB port of the computer and its intensity was regulated with the selector on the LED box (3.5 V was the applied voltage in this work). **Figure S1** shows the integrated SPELEC setup employed for *in situ* dynamic luminescence spectroelectrochemistry with screen-printed electrodes. Luminescence measurements were carried out with an integration time of 2 s unless otherwise stated (one complete spectrum is recorded every 2 s). UV/VIS absorption measurements were performed using a cuvette holder (DRP-CUV, DropSens) for 1 cm pathlength cuvettes and a 10 ms integration time. The normalized fluorescence was calculated as the ratio between the intensity and the initial intensity before the spectroelectrochemical experiments.

Screen-printed carbon electrodes (SPCEs) from DropSens (DRP-110) were employed. These devices incorporate a three-electrode configuration printed on a planar ceramic substrate (with dimensions of 3.4 x 1.0 cm). Both working (disk-shaped 4 mm diameter) and counter electrodes are made of carbon inks, whereas the pseudoreference electrode and electric contacts are made of silver. The geometric area of the working electrode is 0.126 cm^2 (current densities were calculated considering the geometric area). The potential values are reported versus the silver pseudoreference electrode. All measurements with SPCEs were carried out at room temperature and using an aliquot of 50 µL of the appropriate solution. SPCEs were connected to the SPELEC instrument through a specific connector (DropSens, DRP-CAST).

Reagents and solutions

Rhodamine 6G (dye content 99%), potassium chloride, sodium hydroxide, urea and lactic acid were purchased from Sigma-Aldrich. Nitric acid (65%) and ammonia solution (28%) were purchased from Merck. Ultrapure water was obtained from a DirectQ purification system from Millipore.

Artificial sweat preparation

Artificial sweat was prepared following the British Standard (BS EN1811-1999) and according to previous literature[49] but

with two different chloride concentrations. The solution contained 0.12%(w/v) of lactic acid and 0.13%(w/v) of urea. The pH of the solution was adjusted to pH 6.5 using an aqueous solution of ammonia. One artificial sweat sample was prepared with 20 mM of Cl^- and the other one with 93 mM of Cl^-. These concentrations were chosen considering the reference levels for diagnostic of cystic fibrosis in adults: less than 40 mM (negative), 40-59 mM (possible) and greater than 60 mM (positive)[50] with slightly lower values for infants. The sweat samples were used just after the preparation and the sample with highest concentration was diluted 1:4 in order to match with the linear range of the method. For the standard addition method, a 1:1 dilution of artificial sweat was prepared with 0.1 M HNO_3 and increasing concentrations of KCl.

Computational software

The distribution of chlorine-based species in function of pH was estimated by using the open source software package phCalc[51]. This software uses a systematic method to calculate the concentration of chemical species at equilibrium, described in detail in the literature[52].

RESULTS AND DISCUSSION

Spectroscopic and electrochemical behaviour of R 6G

Rhodamine 6G (chemical structure in **Figure S2**) shows interesting optical properties as can be observed in **Figure 1A**, where the absorption and emission spectra are represented. As expected, based on previous studies[53], two main absorption bands with wavelength maxima at about 345 and 522 nm and one emission band at about 554 nm were obtained. The absorption bands could be assigned to the S3→S0 and S1→S0 electronic transitions, respectively[54]. Although the light source employed for emission experiments (LED at λ_{max} =395 nm) is not situated at the absorption maxima, a strong fluorescence intensity was recorded even using a low-concentrated solution (10 µM of R6G) and low integration time (250 ms). A light source nearer to the absorption maximum could increase the fluorescence intensity but the experimental setup needed to discriminate the excitation and the emission radiation would be more complicated. In that case, a complex spectroelectrochemical cell with 45 or 90º arrangement between the excitation and emission lights is mandatory[55], which it is not easily feasible using screen-printed electrodes with a µL-drop configuration. Therefore, the selection of the experimental and instrumental conditions was adequate to obtain a strong R6G emission radiation in conjunction to use a simple instrumental setup.

Although it has been previously suggested that R6G electrochemistry possesses little electrochemical activity[53], the electrochemical behavior on screen-printed carbon electrodes showed different processes. Typical voltammetric curves at 50 mV s^{-1} for increasing bulk concentrations are presented in **Figure 1B**. An initial anodic process was observed in presence of R6G with a peak potential at about +0.85 V, whose intensity increased with the R6G concentration. There are some previous studies on the electrochemical oxidation of Rhodamine dyes, particularly for degradation processes. Although numerous products could be ultimately generated depending on the conditions if a strong rupture of the molecule is achieved, it has been proposed that pathways as the N-deethylation or the cleavage of the chromophore are the most readily produced[56,57]. In a systematic study with similar-structure dyes, Sun et al. proposed that the oxidation may occur at the C=N group that connects the benzene ring as they only found an oxidation process in dyes with this kind of groups[58]. This oxidation process would diminish the delocalization of electrons into the xanthene structure and definitely would have some influence on spectroscopic properties.

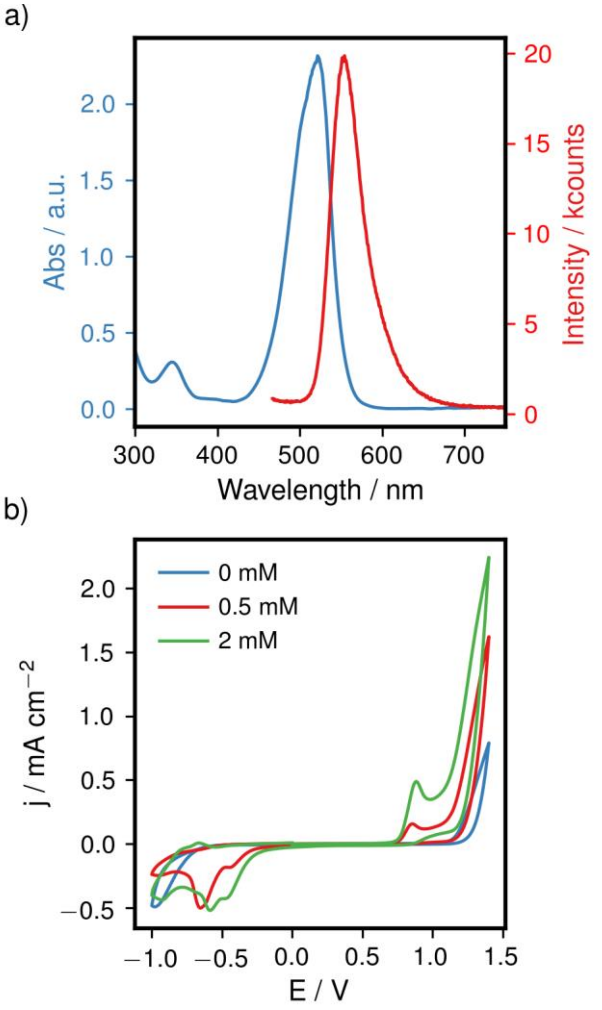

Figure 1. a) UV/VIS (blue line) and emission (red line) spectra for 10 µM R6G in 0.01 M KCl. UV/VIS spectrum was recorded with an integration time of 10 ms and the emission spectra was recorded using a 395 nm LED as excitation source and an integration time of 250 ms. **b)** Cyclic voltammograms obtained for several concentrations of R6G (0, 0.5 and 2 mM) in 0.01 M KCl at screen-printed carbon electrodes. Scan rate of 50 mV s^{-1}.

Another anodic process was observed at the positive edge of the voltammetric curves. Interestingly, the intensity of this process increased with higher R6G concentrations, but it was also visible for the blank solution. The latter fact together with the high currents generated (hundreds of microamps) discards completely the assignment of this process to another R6G oxidation process and it may well be the electrolyte oxidation. Although water oxidation is thermodynamically more favorable than chloride oxidation (see **equations 1-3** for specific standard reduction potentials), the overpotential of water oxidation needed in carbon electrodes is considerably high. Therefore, this anodic process could be tentatively assigned to chloride oxidation. To confirm this hypothesis, cyclic voltammograms with different chloride concentrations were recorded between 0 and +1.6 V (**Figure S3**). As expected, an increasing anodic current was observed with higher chloride concentrations above 1 V, which demonstrates the influence of chloride in the voltammetric curves.

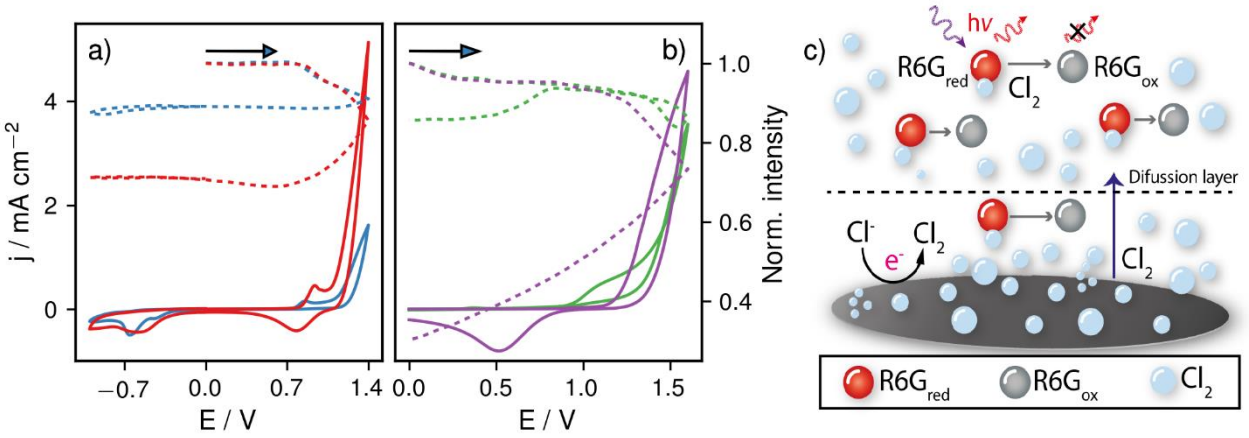

Figure 2. a) Cyclic voltammogram (solid lines) and evolution of the normalized fluorescence intensity (dashed lines) for solutions of 0.5 mM R6G in different concentrations of KCl: 0.01 M (blue line) and 0.1 M (red line). **b)** Cyclic voltammograms (solid lines) and evolution of the normalized fluorescence intensity (dashed lines) for solutions of 10 µM R6G with 0.1 M KCl in different electrolytes: 50 mM HNO_3 (purple line) and 0.1 M NaOH (green line). **c)** Illustrative schematic of the bleaching process after the electrogeneration of gaseous Cl_2 species. Cl_2 bubbles are detached from the electrode surface to the bulk solution where they react with R6G. The initial luminescent reduced R6G ($R6G_{red}$) is oxidized to a non-luminescent product ($R6G_{ox}$).

It is noticeable that in presence of R6G, the chloride oxidation was especially favorable: the currents were higher and the onset potential was lower than in absence of R6G. These symptoms agree well with a possible coupled chemical reaction between the R6G and some product from the chloride oxidation that would regenerate quickly the initial chloride on the electrode surface, avoiding its depletion from the diffusion layer. This mechanism is the typically called catalytic EC' reaction[59] and a proposed simplified equation is shown in **equations 4-5**. However, it is difficult to know if both the initial R6G product and its oxidation product participate in the coupled chemical reaction. The cathodic processes observed in the voltammetric curves were also dependent on the concentration of R6G but they are discussed in the Supporting Information (**Figures S4** and **S5**) due to the lower interest for the main aim of this work.

$$Cl_2 + 2\,e^- \rightleftarrows 2\,Cl^-; \quad E^0 = +1.358\,V \quad (\mathbf{1})$$

$$HClO + H^+ + 2\,e^- \rightleftarrows Cl^- + H_2O; \quad E^0 = +1.482\,V \quad (\mathbf{2})$$

$$O_2 + 4\,H^+ + 4\,e^- \rightleftarrows 2\,H_2O; \quad E^0 = +1.229\,V \quad (\mathbf{3})$$

$$2\,Cl^- \rightleftarrows Cl_2 + 2\,e^- \quad (\mathbf{4})$$

$$R6G_{red} + Cl_2 \rightleftarrows 2\,Cl^- + R6G_{ox} \quad (\mathbf{5})$$

Dynamic spectroelectrochemical study of Rhodamine 6G fluorescence

It is well known that the bleaching activity of chlorine species can be used for degrading or discolorating different dyes[45,46]. We considered the possibility to bleach R6G by *in situ* electrogeneration of chlorine-based species at screen-printed electrodes. The bleaching process was monitored using real-time *in situ* dynamic luminescence spectroelectrochemistry, which allowed us to get continuous and simultaneous electrochemical and optical information during the experiment. Two spectroelectrochemical experiments were performed with two different chloride concentrations (10 and 100 mM). As shown in **Figure 2a**, there was a slight decrease in fluorescence intensity at 554 nm at a potential about +0.90 V. This decrease could be due to the electrochemical oxidation of R6G resulting in a non-fluorescent product and it seems similar in both experiments (similar slopes), which agrees with this possibility as the R6G concentration was the same. Therefore, this oxidation could be decreasing the electronic delocalization on the molecule as previously mentioned, varying the molecular energy levels and removing the strong fluorescence at 554 nm. This change of optical properties is common in different xanthene dyes[43,47], therefore, it seems reasonable to think that the oxidation could be produced in the xanthene group or affect its resonance. Interestingly, when chloride oxidation took place (after +1.0 V), the fluorescence intensity continued decreasing but the rate was remarkably higher for the most concentrated chloride solution and the normalized intensity was lower at the end. Therefore, the bleaching process of R6G by chlorine species can be *in situ* produced by electrochemical techniques and can be monitored by following the optical changes in real-time. It is worth noting that with the configuration employed (long optical path), the fluorescence is recorded from all the solution and not just from the electrode surface. This fact is the main reason as the intensity changes are not complete in a quick experiment like a cyclic voltammetry (the electrolysis is not complete). However, with this setup is possible to monitor chemical reactions occurring in the bulk solution if gas bubbles are generated at the electrode surface and they quickly diffuse towards the solution (*vide infra*).

Chloride oxidation could result in different products depending on the experimental conditions[43] due to the possible disproportionation of chlorine to chloride and hypochlorite/hypochlorous acid as shown in **Equations 6-7**. Using the relative equilibrium constants of chlorine[60], the species distribution as function of pH was estimated (**Figure S6)** and it is in agreement with previous results[43]. Cl_2 is most stable at low pH because the disproportionation reaction would be shifted towards the reagents (Le Chatelier's principle). In an environment with a low H^+ concentration (high pH), this reaction would be shifted

towards the products as the generated H^+ are consumed by the great amount of OH^- in solution, with the ultimate case being the equation 7. HClO species would be mostly in anionic form ClO^- at high pH, with the protonated form HClO being the most predominant species in mild environments. To investigate the species responsible of the fluorescence loss during the electrooxidation of chloride at the electrode surface, dynamic spectroelectrochemical experiments at two extreme pH were carried out. A cyclic voltammetry between 0 and +1.6 V was performed using a 0.1 M NaOH and 0.1 M HNO_3. Chloride and R6G concentrations were the same in both experiments: 100 mM and 10 µM, respectively. **Figure 2b** shows the fluorescence evolution, represented by the normalized intensity, during the dynamic experiment. In the alkaline solution, the fluorescence loss was almost negligible at this range of potentials but in the acidic solution, the fluorescence decreased significantly and continuously from +1.2 V until the end of the experiment. These results clarify the bleaching process by the electrogenerated species: Cl_2, expected in acidic solutions, is the species responsible of the bleaching with a low influence by OCl^-, and the generation of gaseous Cl_2 is able to decrease the fluorescence of the bulk solution as it is demonstrated by the steady loss even at potentials where chloride is not oxidized (below +1.2 V in the reverse scan). If some HOCl were also formed at the electrode surface in the acidic solution, it would be soluble in the solution and the diffusion would be significantly slower compared to gaseous Cl_2. In the timescale of the experiment is not feasible that soluble species diffused as far as expected for the strong decrease in fluorescence observed. Therefore, it seems clear that most of the bleaching is due to the generation and growth of Cl_2 bubbles and its fast detachment from the electrode surface to the solution. A schematic diagram of this process is presented in **Figure 2c**.

$$Cl_2 + H_2O \rightleftarrows HClO + Cl^- + H^+ \quad (6)$$

$$Cl_2 + 2\,OH^- \rightarrow Cl^- + ClO^- + H_2O \quad (7)$$

Spectroelectrochemical experiments using chronoamperometry were performed in order to enhance the electrogeneration of chlorine species by applying a high overpotential (+1.8 V) for 60 s. The evolution of the R6G fluorescence during the experiment with different chloride concentrations (10, 100 mM) in acidic medium (50 mM HNO_3) is shown in **Figure 3a**. The fluorescence decreased for all the solutions, but the rate was slower for lower chloride concentrations. For higher chloride concentrations, a plateau for the bleaching was observed before the experiment was finished, which was due to the complete loss of fluorescence from the solution (**Figure S7**). Again, this fact is in agreement with the bleaching performed by gaseous species and not for soluble species in the solution, which at most it could diffuse about 520 µm from the electrode surface (see Supporting Information for discussion) in the timescale of the experiment (and the thickness of the total solution is about 3 mm). These calculations imply that diffusion is the main mode of mass transport. It must be considered that the generation of bubbles on the electrode would introduce a hydrodynamic component enhancing the mass transport, and therefore, some influence of the soluble species in the bleaching of the bulk solution cannot be discarded. But in that case, it is also directly related to the generation of Cl_2 on the electrode surface during the electrochemical reaction. The fluoresence evolution was dependent on the initial chloride concentration, and therefore, it could be used for chloride quantification (*vide infra*)..

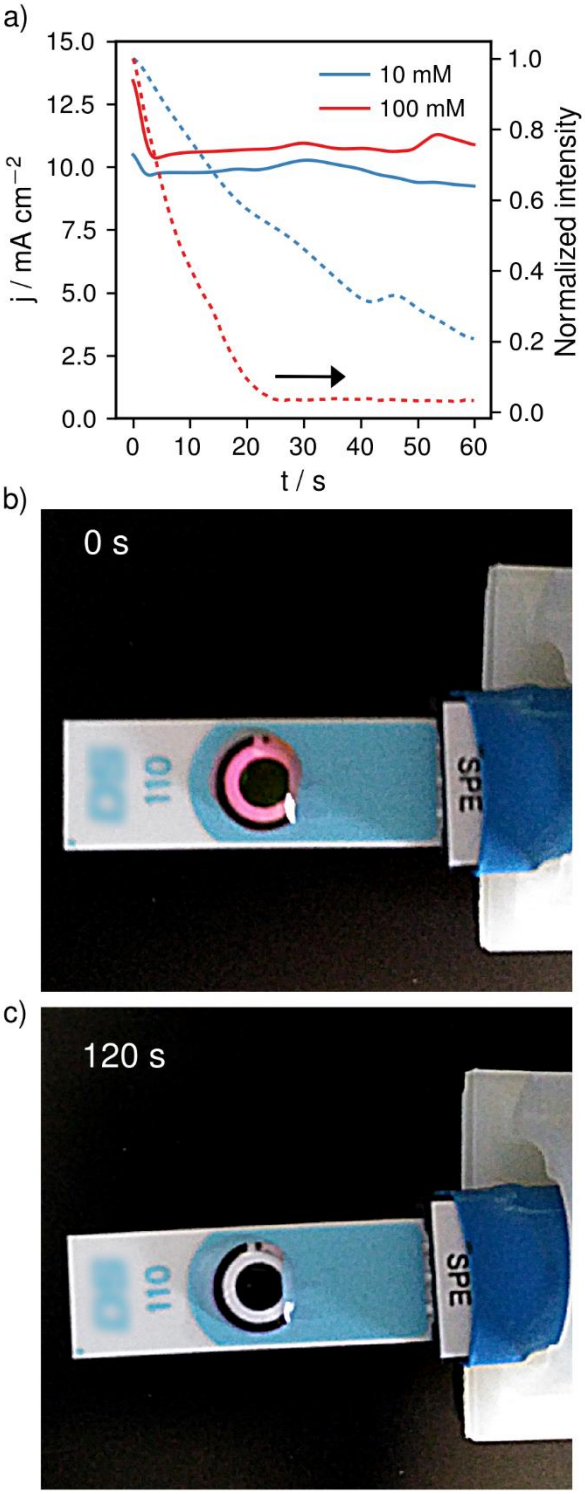

Figure 3. a) Evolution of the normalized fluorescence at 554 nm of 10 µM R6G (dashed lines) during the chronoamperometric experiment (solid lines) for solutions with 10 and 100 mM of KCl. Applied potential was +1.8 V and the electrolyte was 50 mM HNO_3. **b)** Picture of a solution of 90 µM of R6G in 50 mM HNO_3 and 0.4 M KCl. **c)** Picture of the same solution after applying +1.8 V for 120 s.

This fact contrasted with the electrochemical measurements: the currents obtained were not strongly related to the chloride concentration as can be observed in **Figure 3a**, and therefore,

under these experimental conditions, the spectroelectrochemical measurements are essential in order to quantify chloride in the solution. Interestingly, the bleaching of the solution, which is responsible for the fluorescence loss, can also be visually observed during the experiment. **Figures 3b and 3c** show a real picture of the initial solution (90 µM R6G in 50 mM HNO_3 and 0.4 M KCl) and the same solution after the application of +1.8 V for 120 s. The complete experiment is shown in **Video S1** (at 4x speed). The solution with a strong pink color due to the initial R6G lost the color and became a totally transparent solution. Gas bubbles are generated during the process, which could be due to the chlorine electrogenerated at the electrode surface. These bubbles quickly and randomly diffuse to the bulk solution and then enable the reaction between chlorine and R6G, which transforms the colored species to transparent non-fluorescent products.

Quantitative detection of chloride by bleaching of R6G

Spectroelectrochemical methods can be employed for analytical purposes using the change on the optical response related to the analyte concentration[34,39]. In this work, we used the evolution of the R6G fluorescence after the *in situ* electrogeneration of chlorine species, which acted as a fluorescence bleacher.

For the quantification of chloride, a chronoamperometry was performed (+1.8 V) because the bleaching can be enhanced in comparison to a dynamic voltammetry experiment as was previously demonstrated. The experiment was performed for 30 s, but the fluorescence intensity at 25 s was chosen as analytical signal as a compromise in order to be able to differentiate the chloride concentrations and increase the sensitivity. **Figure 4** shows the normalized fluorescence spectra for different chloride concentrations at the beginning of the experiment and at 25 s.

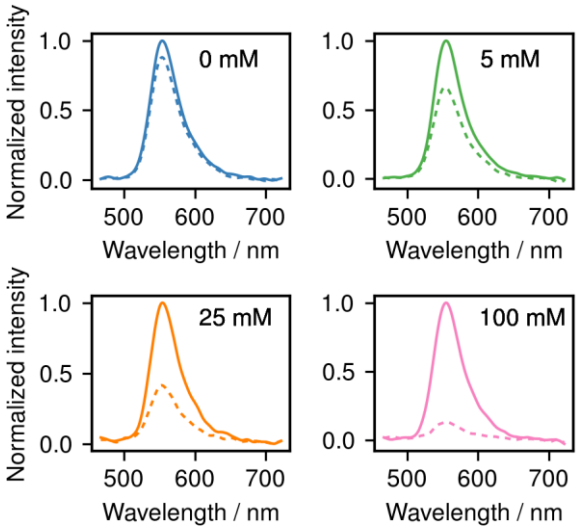

Figure 4. Normalized fluorescence spectra obtained at the beginning of the experiments to record the calibration plot (solid lines) and after 25 s applying +1.8 V (dashed lines) for different chloride concentrations. Solutions were prepared in 50 mM HNO_3.

As expected, the normalized fluorescence decreased significantly with increasing chloride concentrations. The calibration curve for the detection of chloride is presented in **Figure 5**. The behavior of the fluorescence loss is similar to that of static quenching[16], although in this case the quenching is totally irreversible due to the species degradation. Therefore, the concentration response can be described with an equation similar to static quenching:

$$F^0/_F = K_s[Cl^-] + 1 \quad (8)$$

where F_0 is the initial fluorescence of the solution, F is the fluorescence at 25 s (after electrogeneration of chlorine) and K_s is the quenching constant. The linear range of the curve was from 1 to 100 mM of chloride with an equation F^0/F = 0.071 (±0.002) [Cl^-] + 1.04 (±0.08) (n = 3, R^2=0.995). The limit of detection was estimated to be 0.6 mM (S/N=3) and a precision of 7.8% (RSD) was obtained for five replicates (50 mM Cl^-). The generation of Cl_2 bubbles on the electrode surface is somewhat random and that may influence the reproducibility between measurements. A lower precision was found at higher concentrations where the bubbles generation is enhanced (for instance, see Figure 5). However, we consider that the obtained precision is good enough taking into account the use of hyphenated techniques and the low control of the generated bubbles. **Table S1** shows the analytical figures of merit of some electrochemical sensing devices previously reported in the literature for the determination of chloride ions. In some cases, the limit of detection is lower than our method but those devices were modified with complex structures (chemical films, metal nanoparticles, etc.) that increase the device cost. In this work, we report the detection of chloride using low-cost, bare carbon screen-printed devices and the obtained analytical figures of merit are appropriate for the chloride detection in sweat samples for the diagnostic of cystic fibrosis. Our method also solves some issues typically found in ISEs: screen-printed devices are cost-effective, small, portable, convenient for POC analysis, robust and disposable avoiding cleaning steps or the contamination of selective membranes.

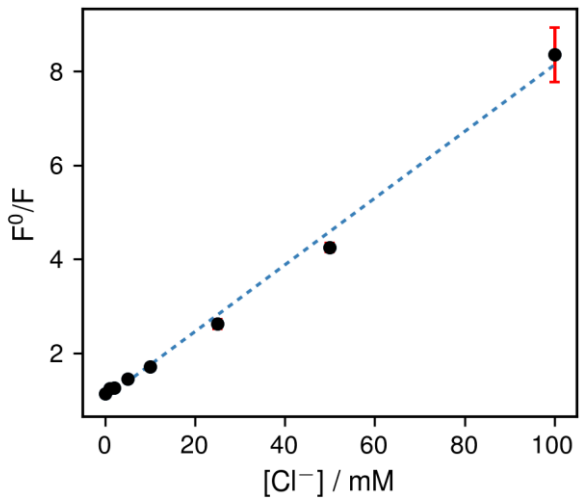

Figure 5. Calibration curve of the ratio between the initial fluorescence and the fluorescence at 25 s of the spectroelectrochemical experiment versus the initial chloride concentration. Solutions were prepared in 50 mM HNO_3.

To demonstrate the applicability of the spectroelectrochemical method, chloride detection in artificial sweat was performed. Two samples of artificial sweat were produced following the British Standard (BS EN1811-1999) but with two

different chloride concentrations: 20 mM and 93 mM. As mentioned, these concentrations were chosen considering the typical reference levels for the diagnostic of cystic fibrosis in adults[50]. The artificial sweat was diluted to obtain final solutions in 50 mM HNO_3 with increasing KCl concentrations. Then, the concentration of chloride in these samples was estimated by using the method of standard addition and the spectroelectrochemical measurement (+1.8 V for 30 s). **Figure 6** shows the standard addition curves obtained for the two samples, and the estimated chloride concentrations were 19 ± 3 and 96 ± 7 mM, respectively. These results demonstrate the good accuracy of the spectroelectrochemical method for the detection of chloride in sweat samples.

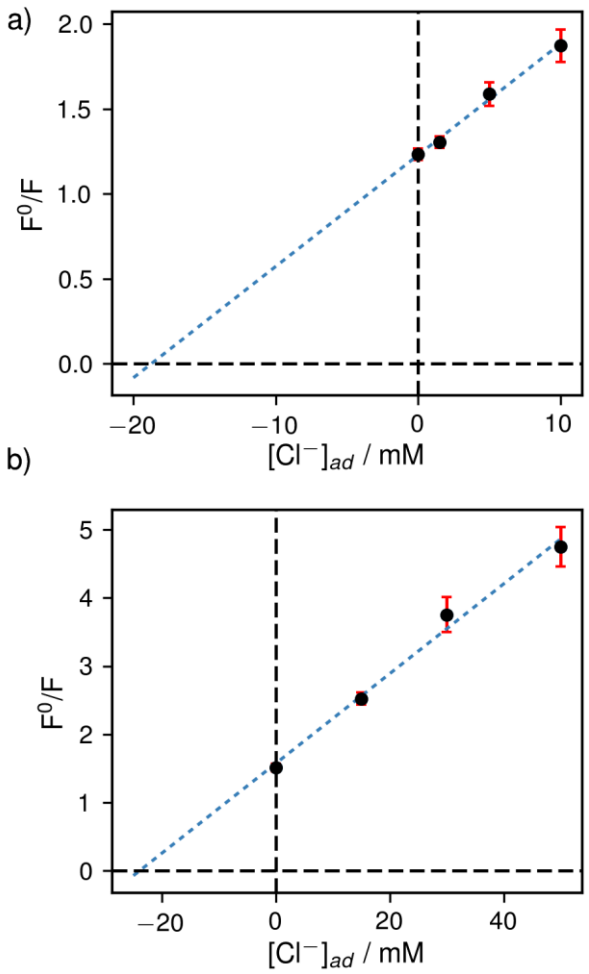

Figure 6. Standard addition curves for the artificial sweat samples: a) low-concentrated sample and b) high-concentrated sample (with a 1:4 dilution). The intersect with y = 0 gives the concentration of the analyzed solution.

CONCLUSIONS

This work has demonstrated how spectroelectrochemistry is a powerful technique for the indirect detection of species that could be difficult to detect directly by electrochemical techniques or with non-significant optical properties. The electrochemical degradation of dyes can be applied for analytical purposes and can be monitored with in situ spectroelectrochemical methods. The generation of gaseous Cl_2 after chloride oxidation seems to induce the quick and severe bleaching of R6G and a fluorescence loss. The change in fluorescence could be correlated with the initial chloride concentration in the solution. Luminescence spectroelectrochemistry was applied to track the optical changes with the final aim of the detection of chloride in artificial samples due to its clinical importance. This approach could be employed with other spectroelectrochemical techniques (UV/VIS, Raman, direct-eye detection), optical probes or chemical species in order to solve different complex analytical problems.

ASSOCIATED CONTENT

Supporting Information

The Supporting Information is available free of charge on the ACS Publications website.

Picture of the spectroelectrochemical instrument, additional voltammetric curves, chlorine species distribution in function of pH, evolution of fluorescence spectra with different chloride concentration, calculations of the thickness of the diffusion layer and standard addition curves for chloride determination (PDF).

Movie showing the bleaching of the R6G solution during a chronoamperometric experiment (MP4).

AUTHOR INFORMATION

Corresponding Author

* Pablo Fanjul-Bolado: pfanjul@dropsens.com

Author Contributions

All authors have given approval to the final version of the manuscript.

REFERENCES

(1) Collins, F. Cystic Fibrosis: Molecular Biology and Therapeutic Implications. *Science (80-.).* **1992**, *256* (5058), 774–779.

(2) Quinton, P. M. Chloride Impermeability in Cystic Fibrosis. *Nature* **1983**, *301* (5899), 421–422.

(3) Dong, H.; Zhang, L.; Liu, W.; Tian, Y. Label-Free Electrochemical Biosensor for Monitoring of Chloride Ion in an Animal Model of Alzhemier's Disease. *ACS Chem. Neurosci.* **2017**, *8* (2), 339–346.

(4) Doorn, J.; Storteboom, T.; Mulder, A.; de Jong, W.; Rottier, B.; Kema, I. Ion Chromatography for the Precise Analysis of Chloride and Sodium in Sweat for the Diagnosis of Cystic Fibrosis. *Ann. Clin. Biochem.* **2015**, *52* (4), 421–427.

(5) LeGrys, V. A.; Yankaskas, J. R.; Quittell, L. M.; Marshall, B. C.; Mogayzel, P. J. Diagnostic Sweat Testing: The Cystic Fibrosis Foundation Guidelines. *J. Pediatr.* **2007**, *151* (1), 85–89.

(6) Arnold, M. A.; Solsky, R. L. Ion-Selective Electrodes. *Anal. Chem.* **1986**, *58* (5), 84–101.

(7) Shishkanova, T. V.; Sýkora, D.; Sessler, J. L.; Král, V. Potentiometric Response and Mechanism of Anionic Recognition of Heterocalixarene-Based Ion Selective Electrodes. *Anal. Chim. Acta* **2007**, *587* (2), 247–253.

(8) Álvarez-Romero, G. A.; Ramírez-Silva, M. T.; Galán-Vidal, C. A.; Páez-Hernández, M. E.; Romero-Romo, M. A. Development of a Chloride Ion-Selective Solid State Sensor Based on Doped Polypyrrole-Graphite-Epoxy Composite. *Electroanalysis* **2010**, *22* (14), 1650–1654.

(9) Dimeski, G.; Badrick, T.; John, A. S. Ion Selective Electrodes (ISEs) and interferences—A Review. *Clin. Chim. Acta* **2010**, *411*

(5–6), 309–317.
(10) Zdrachek, E.; Bakker, E. Time-Dependent Determination of Unbiased Selectivity Coefficients of Ion-Selective Electrodes for Multivalent Ions. *Anal. Chem.* **2017**, *89* (24), 13441–13448.
(11) Michalska, A. All-Solid-State Ion Selective and All-Solid-State Reference Electrodes. *Electroanalysis* **2012**, *24* (6), 1253–1265.
(12) Hu, J.; Stein, A.; Bühlmann, P. Rational Design of All-Solid-State Ion-Selective Electrodes and Reference Electrodes. *TrAC Trends Anal. Chem.* **2016**, *76*, 102–114.
(13) Tian, R.; Qu, Y.; Zheng, X. Amplified Fluorescence Quenching of Lucigenin Self-Assembled inside Silica/Chitosan Nanoparticles by Cl –. *Anal. Chem.* **2014**, *86* (18), 9114–9121.
(14) Kim, J. P.; Xie, Z.; Creer, M.; Liu, Z.; Yang, J. Citrate-Based Fluorescent Materials for Low-Cost Chloride Sensing in the Diagnosis of Cystic Fibrosis. *Chem. Sci.* **2017**, *8* (1), 550–558.
(15) Ruedas-Rama, M. J.; Orte, A.; Hall, E. A. H.; Alvarez-Pez, J. M.; Talavera, E. M. A Chloride Ion Nanosensor for Time-Resolved Fluorimetry and Fluorescence Lifetime Imaging. *Analyst* **2012**, *137* (6), 1500–1508.
(16) Geddes, C. D. Optical Halide Sensing Using Fluorescence Quenching: Theory, Simulations and Applications - a Review. *Meas. Sci. Technol.* **2001**, *12* (9), R53–R88.
(17) Villagrán, C.; Banks, C. E.; Hardacre, C.; Compton, R. G. Electroanalytical Determination of Trace Chloride in Room-Temperature Ionic Liquids. *Anal. Chem.* **2004**, *76* (7), 1998–2003.
(18) Ge, R.; Allen, R. W. K.; Aldous, L.; Bown, M. R.; Doy, N.; Hardacre, C.; MacInnes, J. M.; McHale, G.; Newton, M. I. Evaluation of a Microfluidic Device for the Electrochemical Determination of Halide Content in Ionic Liquids. *Anal. Chem.* **2009**, *81* (4), 1628–1637.
(19) Salehniya, H.; Amiri, M.; Marken, F. Voltammetric Chloride Sensing Based on Trace-Level Mercury Impregnation Into Amine-Functionalized Carbon Nanoparticle Films. *IEEE Sens. J.* **2017**, *17* (17), 5437–5443.
(20) Cuartero, M.; Crespo, G. A.; Bakker, E. Paper-Based Thin-Layer Coulometric Sensor for Halide Determination. *Anal. Chem.* **2015**, *87* (3), 1981–1990.
(21) Cuartero, M.; Crespo, G. A.; Ghahraman Afshar, M.; Bakker, E. Exhaustive Thin-Layer Cyclic Voltammetry for Absolute Multianalyte Halide Detection. *Anal. Chem.* **2014**, *86* (22), 11387–11395.
(22) Giovanni, M.; Pumera, M. Size Dependant Electrochemical Behavior of Silver Nanoparticles with Sizes of 10, 20, 40, 80 and 107 Nm. *Electroanalysis* **2012**, *24* (3), 615–617.
(23) Toh, H. S.; Batchelor-McAuley, C.; Tschulik, K.; Compton, R. G. Electrochemical Detection of Chloride Levels in Sweat Using Silver Nanoparticles: A Basis for the Preliminary Screening for Cystic Fibrosis. *Analyst* **2013**, *138* (15), 4292–4297.
(24) Chiu, M.-H.; Cheng, W.-L.; Muthuraman, G.; Hsu, C.-T.; Chung, H.-H.; Zen, J.-M. A Disposable Screen-Printed Silver Strip Sensor for Single Drop Analysis of Halide in Biological Samples. *Biosens. Bioelectron.* **2009**, *24* (10), 3008–3013.
(25) Bujes-Garrido, J.; Arcos-Martínez, M. J. Disposable Sensor for Electrochemical Determination of Chloride Ions. *Talanta* **2016**, *155*, 153–157.
(26) Lai, S. C. S.; Lazenby, R. A.; Kirkman, P. M.; Unwin, P. R. Nucleation, Aggregative Growth and Detachment of Metal Nanoparticles during Electrodeposition at Electrode Surfaces. *Chem. Sci.* **2015**, *6* (2), 1126–1138.
(27) Zhai, Y.; Zhu, Z.; Zhou, S.; Zhu, C.; Dong, S. Recent Advances in Spectroelectrochemistry. *Nanoscale* **2018**, *10* (7), 3089–3111.
(28) Ramesha, G. K.; Sampath, S. Electrochemical Reduction of Oriented Graphene Oxide Films: An in Situ Raman Spectroelectrochemical Study. *J. Phys. Chem. C* **2009**, *113* (19), 7985–7989.
(29) Barrera, J.; Ibañez, D.; Heras, A.; Ruiz, V.; Colina, A. In-Situ Evidence of the Redox-State Dependence of Photoluminescence in Graphene Quantum Dots. *J. Phys. Chem. Lett.* **2017**, *8* (2), 531–537.
(30) Martín-Yerga, D.; Pérez-Junquera, A.; Hernández-Santos, D.; Fanjul-Bolado, P. Time-Resolved Luminescence Spectroelectrochemistry at Screen-Printed Electrodes: Following the Redox-Dependent Fluorescence of [Ru(bpy) 3] 2+. *Anal. Chem.* **2017**, *89* (20), 10649–10654.
(31) Martín-Yerga, D.; Pérez-Junquera, A.; Hernández-Santos, D.; Fanjul-Bolado, P. Electroluminescence of [Ru(bpy) 3] 2+ at Gold and Silver Screen-Printed Electrodes Followed by Real-Time Spectroelectrochemistry. *Phys. Chem. Chem. Phys.* **2017**, *19* (34), 22633–22637.
(32) Blubaugh, E. A.; Yacynych, A. M.; Heineman, W. R. Thin-Layer Spectroelectrochemistry for Monitoring Kinetics of Electrogenerated Species. *Anal. Chem.* **1979**, *51* (4), 561–565.
(33) González-Diéguez, N.; Colina, A.; López-Palacios, J.; Heras, A. Spectroelectrochemistry at Screen-Printed Electrodes: Determination of Dopamine. *Anal. Chem.* **2012**, *84* (21), 9146–9153.
(34) Martín-Yerga, D.; Pérez-Junquera, A.; González-García, M. B.; Perales-Rondon, J. V.; Heras, A.; Colina, A.; Hernández-Santos, D.; Fanjul-Bolado, P. Quantitative Raman Spectroelectrochemistry Using Silver Screen-Printed Electrodes. *Electrochim. Acta* **2018**, *264*, 183–190.
(35) Hernández, C. N.; Martín-Yerga, D.; González-García, M. B.; Hernández-Santos, D.; Fanjul-Bolado, P. Evaluation of Electrochemical, UV/VIS and Raman Spectroelectrochemical Detection of Naratriptan with Screen-Printed Electrodes. *Talanta* **2018**, *178*, 85–88.
(36) Zhao, L.; Blackburn, J.; Brosseau, C. L. Quantitative Detection of Uric Acid by Electrochemical-Surface Enhanced Raman Spectroscopy Using a Multilayered Au/Ag Substrate. *Anal. Chem.* **2015**, *87* (1), 441–447.
(37) DiVirgilio-Thomas, J. M.; Heineman, W. R.; Seliskar, C. J. Spectroelectrochemical Sensing Based on Multimode Selectivity Simultaneously Achievable in a Single Device. 6. Sensing with a Mediator. *Anal. Chem.* **2000**, *72* (15), 3461–3467.
(38) Richardson, J. N.; Dyer, A. L.; Stegemiller, M. L.; Zudans, I.; Seliskar, C. J.; Heineman, W. R. Spectroelectrochemical Sensing Based on Multimode Selectivity Simultaneously Achievable in a Single Device. 13. Detection of Aqueous Iron by in Situ Complexation with 2,2‘-Bipyridine. *Anal. Chem.* **2002**, *74* (14), 3330–3335.
(39) Branch, S. D.; Lines, A. M.; Lynch, J.; Bello, J. M.; Heineman, W. R.; Bryan, S. A. Optically Transparent Thin-Film Electrode Chip for Spectroelectrochemical Sensing. *Anal. Chem.* **2017**, *89* (14), 7324–7332.
(40) Andria, S. E.; Seliskar, C. J.; Heineman, W. R. Simultaneous Detection of Two Analytes Using a Spectroelectrochemical Sensor. *Anal. Chem.* **2010**, *82* (5), 1720–1726.
(41) Hoener, B. S.; Byers, C. P.; Heiderscheit, T. S.; De Silva Indrasekara, A. S.; Hoggard, A.; Chang, W.-S.; Link, S.; Landes, C. F. Spectroelectrochemistry of Halide Anion Adsorption and Dissolution of Single Gold Nanorods. *J. Phys. Chem. C* **2016**, *120* (37), 20604–20612.
(42) Zong, C.; Chen, C.-J.; Zhang, M.; Wu, D.-Y.; Ren, B. Transient Electrochemical Surface-Enhanced Raman Spectroscopy: A Millisecond Time-Resolved Study of an Electrochemical Redox Process. *J. Am. Chem. Soc.* **2015**, *137* (36), 11768–11774.
(43) Zheng, Y.-M.; Yunus, R. F.; Nanayakkara, K. G. N.; Chen, J. P. Electrochemical Decoloration of Synthetic Wastewater Containing Rhodamine 6G: Behaviors and Mechanism. *Ind. Eng. Chem. Res.* **2012**, *51* (17), 5953–5960.
(44) Combes, R. D.; Haveland-Smith, R. B. A Review of the Genotoxicity of Food, Drug and Cosmetic Colours and Other Azo, Triphenylmethane and Xanthene Dyes. *Mutat. Res. Genet. Toxicol.* **1982**, *98* (2), 101–243.
(45) Martínez-Huitle, C. A.; Brillas, E. Decontamination of Wastewaters Containing Synthetic Organic Dyes by Electrochemical Methods: A General Review. *Appl. Catal. B Environ.* **2009**, *87* (3–4), 105–145.
(46) Brillas, E.; Martínez-Huitle, C. A. Decontamination of Wastewaters Containing Synthetic Organic Dyes by Electrochemical Methods. An Updated Review. *Appl. Catal. B Environ.* **2015**, *166–167*, 603–643.
(47) Dai, Q.; Jiang, L.; Luo, X. Electrochemical Oxidation of Rhodamine B: Optimization and Degradation Mechanism. *Int. J. Electrochem. Sci.* **2017**, *12* (5), 4265–4276.
(48) FaridaYunus, R.; Zheng, Y.-M.; Nanayakkara, K. G. N.; Chen, J. P. Electrochemical Removal of Rhodamine 6G by Using RuO 2 Coated Ti DSA. *Ind. Eng. Chem. Res.* **2009**, *48* (16), 7466–7473.
(49) Kulthong, K.; Srisung, S.; Boonpavanitchakul, K.;

Kangwansupamonkon, W.; Maniratanachote, R. Determination of Silver Nanoparticle Release from Antibacterial Fabrics into Artificial Sweat. *Part. Fibre Toxicol.* **2010**, *7* (1), 8.
(50) Schulz, I. J. Micropuncture Studies of the Sweat Formation in Cystic Fibrosis Patients. *J. Clin. Invest.* **1969**, *48* (8), 1470–1477.
(51) pHcalc: Systematic pH calculation package https://github.com/rnelsonchem/pHcalc.
(52) Baeza-Baeza, J. J.; García-Álvarez-Coque, M. C. Systematic Approach To Calculate the Concentration of Chemical Species in Multi-Equilibrium Problems. *J. Chem. Educ.* **2011**, *88* (2), 169–173.
(53) Yu, J.-S.; Zhou, T.-Y. The Electrochemistry and Thin-Layer Luminescence Spectroelectrochemistry of Rhodamine 6G at a 4,4′-Bipyridine-Modified Gold Electrode. *J. Electroanal. Chem.* **2001**, *504* (1), 89–95.
(54) Fedoseeva, M.; Letrun, R.; Vauthey, E. Excited-State Dynamics of Rhodamine 6G in Aqueous Solution and at the Dodecane/Water Interface. *J. Phys. Chem. B* **2014**, *118* (19), 5184–5193.
(55) León, L.; Mozo, J. D. Designing Spectroelectrochemical Cells: A Review. *TrAC Trends Anal. Chem.* **2018**.
(56) Singh, S.; Srivastava, V. C.; Mall, I. D. Mechanism of Dye Degradation during Electrochemical Treatment. *J. Phys. Chem. C* **2013**, *117* (29), 15229–15240.
(57) Araújo, D. M. de; Sáez, C.; Martínez-Huitle, C. A.; Cañizares, P.; Rodrigo, M. A. Influence of Mediated Processes on the Removal of Rhodamine with Conductive-Diamond Electrochemical Oxidation. *Appl. Catal. B Environ.* **2015**, *166–167*, 454–459.
(58) Sun, J.; Gan, T.; Li, Y.; Shi, Z.; Liu, Y. Rapid and Sensitive Strategy for Rhodamine B Detection Using a Novel Electrochemical Platform Based on Core–shell Structured Cu@carbon Sphere Nanohybrid. *J. Electroanal. Chem.* **2014**, *724*, 87–94.
(59) Molina, A.; González, J.; Laborda, E.; Wang, Y.; Compton, R. G. Catalytic Mechanism in Cyclic Voltammetry at Disc Electrodes: An Analytical Solution. *Phys. Chem. Chem. Phys.* **2011**, *13* (32), 14694–14704.
(60) Deborde, M.; von Gunten, U. Reactions of Chlorine with Inorganic and Organic Compounds during Water treatment—Kinetics and Mechanisms: A Critical Review. *Water Res.* **2008**, *42* (1–2), 13–51.

Table of Contents artwork

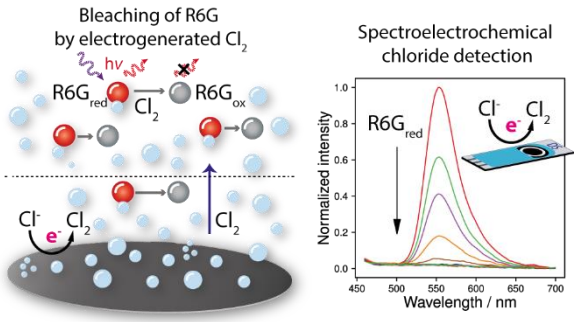

SUPPORTING INFORMATION

In Situ Spectroelectrochemical Monitoring of Dye Bleaching After Electrogeneration of Chlorine-Based Species. Application to Chloride Detection

Daniel Martín-Yerga, Alejandro Pérez-Junquera, María Begoña González-García, David Hernández-Santos, Pablo Fanjul-Bolado*

DropSens, S.L., Ed. CEEI, Parque Tecnológico de Asturias, 33428 Llanera, Asturias, Spain

*Corresponding author: pfanjul@dropsens.com

TABLE OF CONTENTS

S1. Instrumental setup

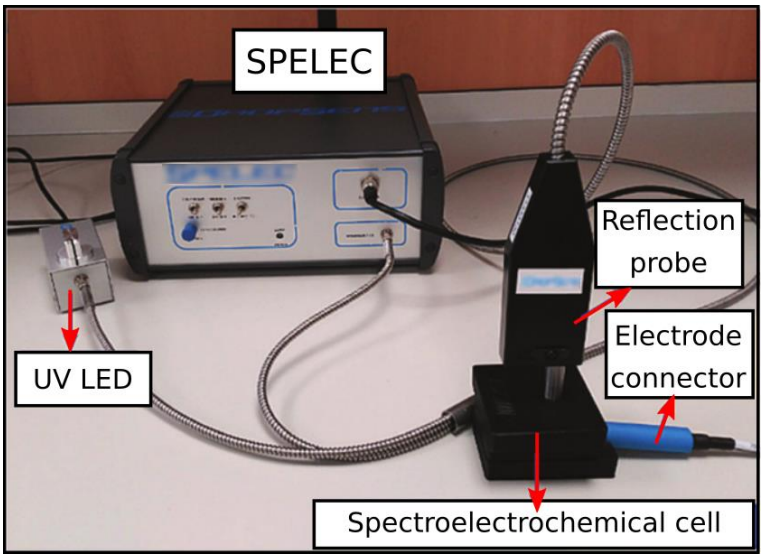

Figure S1. Instrumental setup employed for the luminescence spectroelectrochemistry experiments. The setup integrates the spectroelectrochemical instrument, SPELEC, an UV LED, a reflection probe and a spectroelectrochemical cell for screen-printed electrodes. Optical and electrochemical data are obtained *in situ*, in real-time and with high time-resolution from the same sample.

S2. Chemical structure of Rhodamine 6G

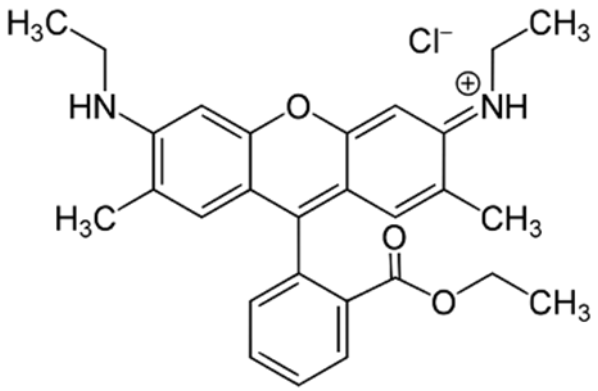

Figure S2. Chemical structure of Rhodamine 6G containing the xanthene group, which characterize this kind of dyes and their optical properties.

S3. Cyclic voltammetry of chloride solutions

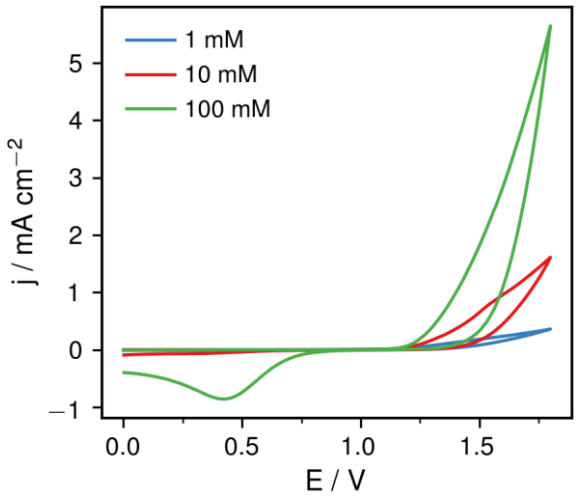

Figure S3. Cyclic voltammograms obtained for solutions of different KCl concentrations (1, 10 and 100 mM). The increasing anodic process is due to the oxidation of chloride to chlorine-based species. For high initial concentrations of chloride, a cathodic process is observed due to the reverse reaction (reduction of oxidized species to chloride). The cathodic peak current is significantly lower that the anodic currents suggesting a low reversibility on the electrochemical reaction, which is possibly due to the deficiency of chlorine at the electrode surface after the release of gas to the bulk solution.

S4. Cyclic voltammetry of Rhodamine 6G at negative potentials

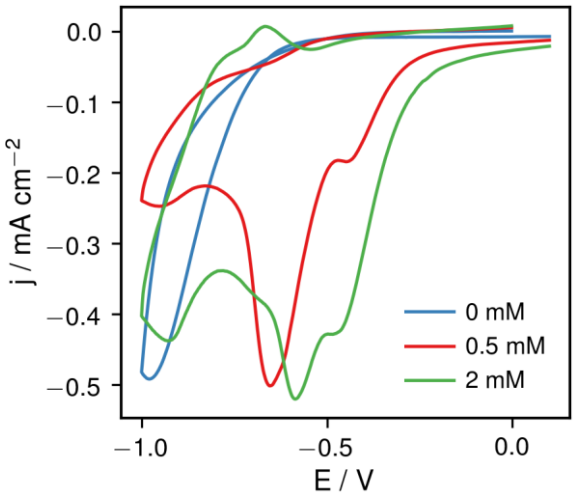

Figure S4. Voltammetric curves for solutions of different R6G concentrations (0, 0.5 and 2 mM) at negative potentials. In absence of R6G a cathodic process is observed c.a. -1.0 V, which could be tentatively assigned to oxygen reduction reaction. However, the most interesting processes appear in the cathodic part between -0.5 and -0.6 V, which are assigned to reduction of R6G. The first process has a clear relation with the R6G concentration, but the magnitude of the second process seems to be constant. This kind of behavior is typically observed for combined adsorption-diffusion processes and that may be the case for R6G at negative potentials. However, it is difficult to assign them due to the low resolution. The mechanism of reduction of xanthene dyes has been previously discussed[1] and it is usually ascribed to the reduction of the carbon atom in the central ring (**Figure S5**)

S5. Proposed reaction for R6G reduction

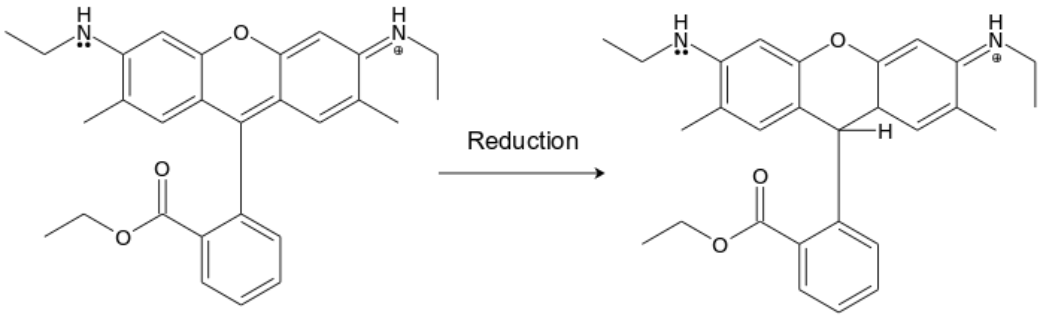

Figure S5. Proposed electrochemical reduction of R6G, similar to other xanthene dyes.

S6. Distribution of chlorine species in function of pH

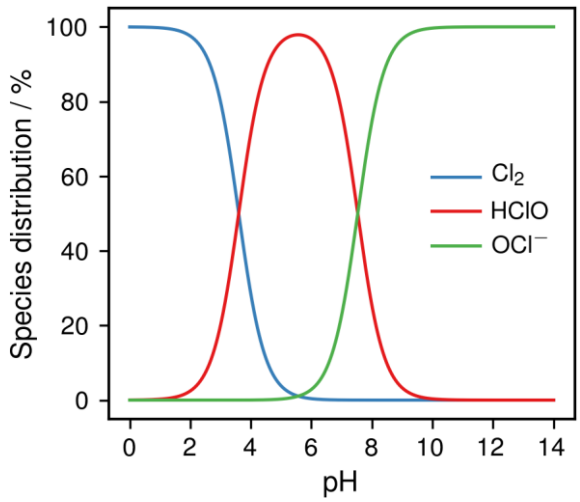

Figure S6. Calculated distribution of chlorine-based species in function of pH.

S7. Fluorescence evolution during spectroelectrochemical experiment

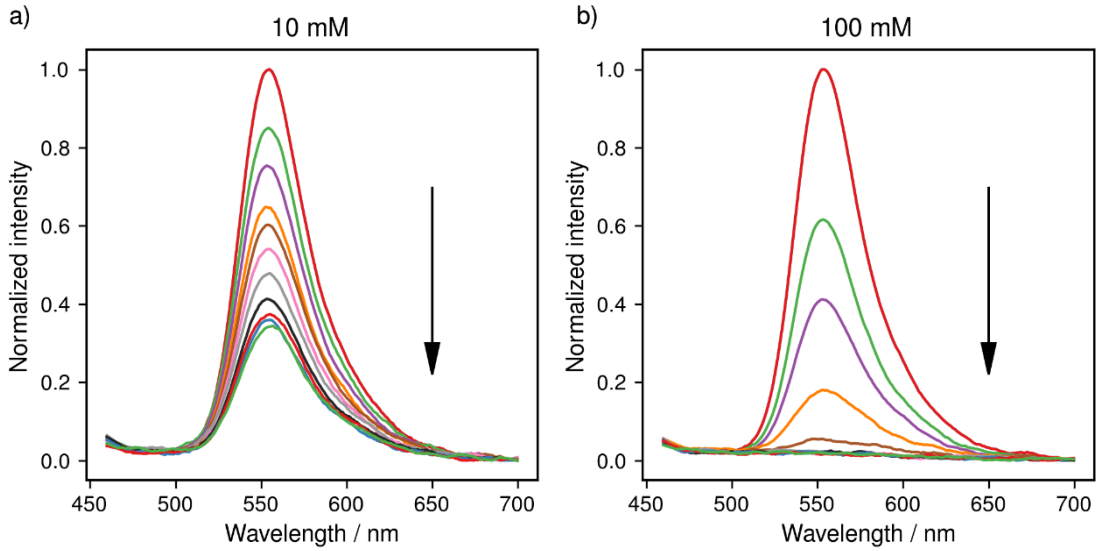

Figure S7. Evolution of the fluorescence spectra during the chronoamperometric spectroelectrochemical experiment for chloride solutions of a) 10 mM and b) 100 mM. Spectra with same color in both figures are recorded at the same time. The rate of decrease was significantly greater for the solution with higher chloride concentration and the final normalized fluorescence was close to zero (baseline). In contrast, for the lower chloride concentration, the rate of decrease was inferior and the final normalized fluorescence was above 0.3, suggesting a limiting generation of the bleaching species.

S8. Estimation of the thickness of the diffusion layer

In order to estimate the distance travelling from the electrode surface of species controlled by diffusion, the thickness of the diffusion layer was calculated. We used 30 s as the time of the experiment because at this time the fluorescence was totally removed from the bulk solution during the chronoamperometric experiments for 100 mM chloride (see **Figure 3** in main manuscript).

The diffusion coefficients for ClO^- or HClO are in the order of 1.5-1.6 x 10^{-5} cm/s as previously discussed in the literature[2].

For a planar macroelectrode under linear diffusion control as expected for screen-printed electrodes, the thickness of the diffusion layer (δ) is proportional to the square root of the diffusion coefficient (D) and the experimental time (t), with the extreme case of the maximum possible thickness given by the following equation[3]:

$$\delta_{max} = \sqrt{6 * D * t}$$

This is a limiting case, and the thickness of the diffusion layer will probably be much lower than this value. The thickness obtained for ClO^- or HClO would be about 0.52 mm at 30 s. This value is far from the thickness of the bulk solution employed in the experiments (about 3 mm), and therefore, if the bleaching of R6G was due to the soluble species controlled by diffusion, it would be computable for the 17% of the bleaching at most. For 100 mM and this experimental time, the 100% of the solution was bleached. This fact demonstrates that the primary process responsible for the bleaching is clearly due to the interaction of chlorine gas with the bulk solution.

S9. Analytical figures of merit of electrochemical devices for the determination of chloride

Table S1. Analytical figures of merit of electrochemical devices for the determination of chloride

Technique	Material	Dynamic range	Limit of detection	Reference
Potentiometry	Ag/AgCl	1 – 6 mM	-	4
Voltammetry	MnO_2/Co_3O_4 nanoparticles	1 – 100 µM	0.35 µM	5
Voltammetry	Ag/AgCl reference electrode	10 – 100 mM	10 mM	6
Voltammetry	Ag ink on filter paper	10 – 200 mM	1 mM	7
Voltammetry	Ag nanoparticles on screen-printed electrodes	2 – 40 mM	-	8
Voltammetry	Ag nanowires / Pt	0.2 – 20.2 mM	20 µM	
Coulometry	Ag foil on Nafion-coated paper	0.01 – 0.6 mM	10 µM	9
Potentiometry	Ion-selective electrode: doped polypyrrole-graphite-epoxy	-	3 µM	10
Potentiometry	Ion-selective electrode: calix[2]pyridino[2]pyrrole receptor	0.01 – 100 mM	-	11
Spectroelectrochemistry	Screen-printed carbon electrodes	1 – 100 mM	0.6 mM	This work

S10. Video caption

Video S1. Movie illustrating the bleaching process of the R6G solution after applying a constant potential (+1.8 V) for 120 s. The concentration of R6G was 90 µM and 0.4 M for NaCl. The movie is at 4x speed.

S10. References

(1) Čížková, M.; Cattiaux, L.; Mallet, J.-M.; Labbé, E.; Buriez, O. Electrochemical Switching Fluorescence Emission in Rhodamine Derivatives. *Electrochim. Acta* **2018**, *260*, 589–597.

(2) Chao, M. S. The Diffusion Coefficients of Hypochlorite, Hypochlorous Acid, and Chlorine in Aqueous Media by Chronopotentiometry. *J. Electrochem. Soc.* **1968**, *115* (11), 1172.

(3) Bard, A. J.; Faulkner, L. R. *Electrochemical Methods: Fundamentals and Applications*, 2nd ed.; John Wiley & Sons, 2001.

(4) de Graaf, D. B.; Abbas, Y.; Gerrit Bomer, J.; Olthuis, W.; van den Berg, A. Sensor–actuator System for Dynamic Chloride Ion Determination. *Anal. Chim. Acta* **2015**, *888*, 44–51.

(5) Rahman, M. M.; Khan, S. B.; Gruner, G.; Al-Ghamdi, M. S.; Daous, M. A.; Asiri, A. M. Chloride Ion Sensors Based on Low-Dimensional α-MnO2–Co3O4 Nanoparticles Fabricated Glassy Carbon Electrodes by Simple I–V Technique. *Electrochim. Acta* **2013**, *103*, 143–150.

(6) Bujes-Garrido, J.; Arcos-Martínez, M. J. Disposable Sensor for Electrochemical Determination of Chloride Ions. *Talanta* **2016**, *155*, 153–157.

(7) Cinti, S.; Fiore, L.; Massoud, R.; Cortese, C.; Moscone, D.; Palleschi, G.; Arduini, F. Low-Cost and Reagent-Free Paper-Based Device to Detect Chloride Ions in Serum and Sweat. *Talanta* **2018**, *179*, 186–192.

(8) Toh, H. S.; Batchelor-McAuley, C.; Tschulik, K.; Compton, R. G. Electrochemical Detection of Chloride Levels in Sweat Using Silver Nanoparticles: A Basis for the Preliminary Screening for Cystic Fibrosis. *Analyst* **2013**, *138* (15), 4292–4297.

(9) Cuartero, M.; Crespo, G. A.; Bakker, E. Paper-Based Thin-Layer Coulometric Sensor for Halide Determination. *Anal. Chem.* **2015**, *87* (3), 1981–1990.

(10) Álvarez-Romero, G. A.; Ramírez-Silva, M. T.; Galán-Vidal, C. A.; Páez-Hernández, M. E.; Romero-Romo, M. A. Development of a Chloride Ion-Selective Solid State Sensor Based on Doped Polypyrrole-Graphite-Epoxy Composite. *Electroanalysis* **2010**, *22* (14), 1650–1654.

(11) Shishkanova, T. V.; Sýkora, D.; Sessler, J. L.; Král, V. Potentiometric Response and Mechanism of Anionic Recognition of Heterocalixarene-Based Ion Selective Electrodes. *Anal. Chim. Acta* **2007**, *587* (2), 247–253.